Air-sea interaction in the Gulf of Guinea at intraseasonal time-scales: wind bursts and coastal precipitation in boreal spring

Marion Leduc-Leballeur, Gaëlle de Coëtlogon, Laurence Eymard

Air–sea interaction in the Gulf of Guinea at intraseasonal time-scales: wind bursts and coastal precipitation in boreal spring

Marion Leduc-Leballeur,[a] Gaëlle de Coëtlogon[a]* and Laurence Eymard[b]
[a]*LATMOS–IPSL, UPMC, Paris, France*
[b]*LOCEAN–IPSL, UPMC, Paris, France*

The role of air-sea interaction in the boreal spring precipitation of the West African monsoon is explored through the wind variability in the Gulf of Guinea. Linear regressions are performed in May-June during the decade 2000-2009 to investigate the origin and effect of the surface wind strengthening north of the equator. It appears that the equatorial sea surface temperature (SST) cooling intensifies a surface wind equatorial divergence / coastal convergence circulation, and generates a cross-equatorial pressure gradient, which both strengthen the southerlies north of the equator. This increases subsidence above the ocean and convection in the northern Gulf of Guinea. In addition, an abrupt change is observed in the surface wind pattern in the eastern equatorial Atlantic (EEA) between April and July. To investigate the transition mechanisms, a reference date is defined as the date when the surface wind north of the equator becomes and remains stronger than south of the equator. Thus, the maintenance of strong southerlies north of the equator is linked to a coincident installation of a deep circulation on the whole troposphere and a northward shift of the low atmospheric local circulation. The resulting sharp seasonal transition coincides each year with a southeasterly wind burst, suggesting that the equatorial SST cooling plays a role in the precipitation along the African coast during boreal spring.

Key Words: West African monsoon; tropical Atlantic

Received 12 August 2011; Revised 25 April 2012; Accepted 2 May 2012

Citation: Leduc-Leballeur M, de Coëtlogon G, Eymard L. 2013. Air–sea interaction in the Gulf of Guinea at intraseasonal time-scales: wind bursts and coastal precipitation in boreal spring. Q. J. R. Meteorol. Soc. 139:387–400. doi:10.1002/qj.1981

1. Introduction

The eastern equatorial Atlantic (EEA) is subject to a strong annual cycle in sea surface temperature (SST), surface wind and deep convection activity (Mitchell and Wallace 1992; Li and Philander 1997; Gu and Adler 2004). In March-April, the InterTropical Convergence Zone (ITCZ) located by the maximum precipitation stands near the equator and SST is uniformly warm in the equatorial zone of 10°S-5°N (Xie and Carton 2004). From April to July, the SST progressively cools between 4°S and 1°N and the precipitation of the West African monsoon is concentrated over the Gulf of Guinea (Gu and Adler 2004). This SST cooling is associated with the development of the equatorial upwelling. Its appearance is mainly due to the intensification of the southeastern trades. However, others processes act, such as horizontal advection (de Coëtlogon *et al.* 2010), oceanic vertical mixing (Peter *et al.* 2006), equatorial Kevin waves (McCreary *et al.* 1984) and oceanic surface currents (Giordani and Caniaux 2011). Several authors suggest an influence of this SST cooling on the beginning of the West African monsoon (Vizy and Cook 2001; Sultan and Janicot 2003; Gu and Adler 2004; Okumura and Xie 2004; Caniaux *et al.* 2011).

At intraseasonal timescales, de Coëtlogon *et al.* (2010) study the air-sea interaction in the Gulf of Guinea. By using linear statistical analyses over 8 years of satellite data (2000-2007), they found a negative feedback between the

SST and the surface wind in the EEA during boreal spring and summer: stronger than normal southeasterlies, controlled by fluctuations of the St Helena anticyclone, lead to an equatorial SST cooling south of the equator. In turn, this cold SST anomaly slows down the overlying wind within a few days. This feedback is found again and detailed for April to July 2006 in Leduc-Leballeur *et al.* (2011). Moreover, the latter note that an acceleration of southeasterlies over the EEA is associated with a local acceleration of southerlies just north of the equator, through the SST front located around 1°N. This surface wind strengthening tends to favour such a coastal convergence, which suggests an influence on coastal precipitations. As Leduc-Leballeur *et al.* (2011) only investigated the year 2006, an extension over the whole 2000-2009 decade motivates a new study.

At the seasonal timescales, Caniaux *et al.* (2011) observe a high correlation between the equatorial upwelling and the West African monsoon onset in the Sahelian region and suggest that it comes from strong interactions between the SST cooling and wind pattern in the EEA: the southeasterlies decelerate south of the equator due to the cold SST and increase further North after crossing the equator due to warmer SST. They conclude that this wind strengthening on the northern side of the equator, from March to mid June, contributes to the northward migration of humidity and convection, and pushes precipitation to the continent. Thorncroft *et al.* (2011) study the water vapour transport towards the African coast. They observe that the key aspect of the rainfall coastal onset is the acceleration of low-level cross-equatorial southerlies, which develops the seasonal equatorial SST cooling and transports moisture towards the coast. They also suggest that the equatorial SST cooling strongly regulates the date and intensity of coastal rainfall in boreal spring. However, the local atmospheric circulation in the Gulf of Guinea remains largely unknown, as well as the mechanisms of the air-sea interaction leading to its intraseasonal variability.

The aim of this study is to identify the interaction mechanisms and their role in the convective enhancement and coastal precipitation observed in the Gulf of Guinea during boreal spring. To achieve this, a focus is made on the May-June period during the decade 2000-2009. Section 2 describes the satellite data and model reanalyses used for this study. In section 3, the origin of the wind strengthening events north of the equator is investigated, as well as their consequences. This phenomenon is then linked to the intraseasonal evolution observed during May-June, in section 4. Finally, a summary and some concluding remarks are provided in section 5.

2. Data

2.1. Satellite measurements

The SST is retrieved from the TMI (Tropical Rainfall Measuring Mission (TRMM) Microwave Imager) (Wentz 1997; Wentz *et al.* 2000), and surface wind vectors are provided by the QuikScat (Quick Scatterometer) satellite (Liu *et al.* 2000), all available on the Remote Sensing Systems website (www.remss.com), as 3-day running mean on a 0.25° x 0.25° grid between 2000 and 2009. A two-dimensional cubic-spline interpolation first filled the gaps due to the clouds for each available day, and then a linear interpolation at each grid point completed the missing days (about only 15 over the whole decade).

In addition, the daily TRMM 3B42 product on a 0.25° x 0.25° grid is used. It mixes satellite measurements with data from ground radars (Huffman *et al.* 2007), which guarantees the best possible quality for precipitation data. It is retrieved from the website trmm.gsfc.nasa.gov.

2.2. Reanalyses

Two reanalyses datasets are used: the ERA-Interim reanalysis from the European Centre for Medium-Range Weather Forecasts (ECMWF) (hereafter ERAI; Dee *et al.* (2011)) and the Climate Forecast System Reanalysis (CFSR; Saha *et al.* (2010)) from the National Centres for Environmental Prediction (NCEP). One of the distinctive CFSR characteristics is the coupling of atmosphere and ocean models, constrained to ERAI, which provides an advantage for the air-sea interaction study.

The reanalyses data are available on a 0.75° x 0.75° horizontal grid for ERAI and 0.5° x 0.5° for CFSR, with vertical atmospheric profiles retrieved on 23 levels from 1000 to 200 hPa for both. For this study, the daily mean of the 6-hourly parameters is used over the decade 2000-2009.

2.3. Study domain

As the processes of interest occur in the Gulf of Guinea, the study focuses on the region east of 10°W. The meridional sections are computed between 10-6°W. Indeed, it is the meridional band where the May-June standard deviation of both SST and surface wind is maximal. In agreement, Leduc-Leballeur *et al.* (2011) observe for the year 2006 that the 10-6°W band maximizes the significance of air-sea interaction effects during boreal spring. However, the same analyses are being realized on the whole 10°W-6°E meridional band to check this and similar results have been found.

3. Impact of wind bursts north of the equator

3.1. Index definition

In this section, linear statistics are used to investigate the evolution of surface and tropospheric parameters, linked to a strengthening of surface wind north of the equator. The recent use of satellite data (starting at the end of 1999 for QuikSCAT) as inputs in reanalysis products improves their quality, which is why only reanalyses starting in 2000 and after are investigated in this study. In particular, the use of only 2 or 3 months per year makes it still possible to obtain a reasonable degree of freedom in time series, authorizing an in-depth study of short periods in the year, such as the boreal spring season, which is critical for the Guinean coast rainfall. Several studies note that it occurs in May-June (Zheng *et al.* 1999; Sultan and Janicot 2003; Gu and Adler 2004; Thorncroft *et al.* 2011). Thorncroft *et al.* (2011) defined May-June as the "coastal phase" of the West African monsoon, when precipitation is maximal over the coastal region (around 5°N), together with an acceleration of southerlies in the low atmosphere. May-June is thus the relevant period to study the effect of surface

wind strengthening events on coastal precipitation. The non-negligible seasonal evolution, which exists during these two months, will be explored in section 4.

From 2000 to 2009, an index (noted V-index hereafter) is built by averaging the 10 m meridional wind (V) in the 1-4°N/10-6°W area (black box in Figure 1) to focus on the surface wind strengthening events north of the equator. This V-index is filtered using a Lanczos high-pass filter with a 1/90-day cutoff to remove the seasonal cycle. The anomaly fields are computed by removing the mean of the May-June period from the original fields. Then, lagged regressions onto the V-index are performed for May-June. The correlations are computed at each grid point between the anomaly fields and the V-index, weighted by the root-mean-square (rms) of the field (according to a widely used method, used by de Coëtlogon *et al.* (2010)). Therefore, regressions show the anomaly pattern linearly correlated with a one standard-deviation anomaly of the V-index. Only correlations above the 10 % significant level are shown (*i.e.* there is less than 10 % chance that the correlation would be random).

The statistical analysis is performed with satellite, ERAI and CFSR datasets and provides a preliminary view of the air-sea interaction and tropospheric events linked to a strengthening of the surface wind north of the equator.

3.2. Air-sea interaction

Figure 1 shows the SST, sea level pressure (SLP) and surface wind in the EEA in May-June, averaged over the decade 2000-2009 as well as the results from the linear regressions performed on the V-index, from lag -2 (*i.e.* 2 days before a stronger-than-normal V-index) to lag 4 (4 days after), for TMI and QuikScat satellites (left), ERAI (centre) and CFSR (right). The satellites products and the two reanalyses exhibit similar patterns, which give a general description of air-sea interactions.

During May-June, the equatorial upwelling develops and a relatively cold SST (about 26°C) lies between the equator and about 3°S. North of the equator, the SST is warmer (about 28°C). A front between these cold and warm waters forms along 1°N with a SST difference about 2°C from side to side. The overlying SLP gradient, of about 0.5 hPa by 300 km, is mainly oriented North-South with a slightly eastward orientation. The highest SLP is located in the southwestern part of the domain (about 1013.5 hPa) and the lowest in the northeast (around 1012 hPa over the ocean). Following this gradient, the overlying winds are mainly directed northward, with an easterly component in the south turning westerly between the equator and the African coast.

At lag -2, linear regressions show a negative SST anomaly around the equator (Figure 1c-d). This cooling persists to lag 4 and is the most intense between 3°W and 9°W at lag 4 (minus 0.4°C in TMI, 0.2°C in ERAI and 0.3°C in CFSR). A general increase in the northward meridional SLP gradient is observed until lag 0, together with the development of southerlies (which are maximal, by definition, at lag 0). From lag 0 onwards, this positive SLP anomaly organises around the negative SST anomaly. This tends to decrease the SLP anomaly gradient south of the equator, and reverses it. Since the cooling in the eastern part of the domain develops after the western one, a zonal gradient of SLP anomaly is even visible in the central part of the domain at lags 1 and 2 in ERAI (from lags 1 to 4 in CFSR). North of the equator, on the contrary, a northward meridional SLP anomaly gradient settles. Most of the wind anomalies observed from lag 0 onwards are consistent with these SLP anomaly gradients: south of the equator, the northward anomalies disappear and become southward together with the inversion of the meridional SLP anomaly gradients, and north of the equator, a northward component persists. Besides, while the western cooling develops earlier than the eastern one, a clear eastward component can be seen in the winds anomaly, in the same direction as the zonal SLP anomaly gradient.

The cooling of the equatorial SST observed after a wind burst agrees with previous studies. Indeed, Marin *et al.* (2009) show the SST seasonal cooling at the equator is not smooth and continued, but results from the succession of short-duration cooling events. These are generated by southeastern wind bursts due to the fluctuating St Helena anticyclone. At this shorter timescale (a few days), de Coëtlogon *et al.* (2010) found that more than half of the cold SST anomaly in the front zone could be explained by horizontal oceanic advection: stronger southerlies create northward surface currents anomaly, which bring northward colder waters around the equator. The SST cooling is thus controlled by the wind with a lag of a few days (due to the relatively large inertia of oceanic currents). This persistence explains why the cooling observed in Figure 1 starts before and persists after lag 0.

In turn, a SST anomaly can influence the overlying surface winds. Indeed, wind acceleration over warmer SST has been observed in the North Atlantic or Pacific (*e.g.* Businger and Shaw 1984; Friehe *et al.* 1991; Kwon *et al.* 1998; Hashizume *et al.* 2002). Two main mechanisms were proposed to explain the influence of a SST front on the wind in the case of wind blowing from cold to warm SST (Xie 2004; Small *et al.* 2008). The first one is linked to the stability of the lower marine atmospheric boundary layer (Sweet *et al.* 1981; Wallace *et al.* 1989): the cold SST tends to decrease the vertical mixing of momentum and thereby weakens the surface wind by mixing it with stronger wind aloft. Conversely, above warm SST, the vertical mixing of momentum tends to increase and thereby strengthen the surface wind. The anomalous wind patterns in Figure 1 illustrate very clearly this effect: as shows their comparison with the mean surface wind patterns (a, b and c), surface winds in the three datasets are actually becoming weaker over the cooling SST, which would increase the stability of the air column. This is consistent with de Coëtlogon *et al.* (2010), who suggest that the mechanism linked to the vertical mixing of momentum play a dominant role in this region. The second mechanism underlines the effects of the SLP gradient induced by the SST front (Lindzen and Nigam 1987): the rapid change in the air temperature and humidity induced by the SST front results in a tight pressure gradient, with a high pressure over the cold temperature and a low pressure over the warm temperature. This is in very good agreement with the evolution of the SLP anomaly pattern seen in Figure 1: around 6°W on the equator, where the SST response to the wind is the strongest, the positive SLP anomaly induced by the SST cooling can be seen to decrease the local SLP gradient as early as lag 0. From lag 2 onwards, the

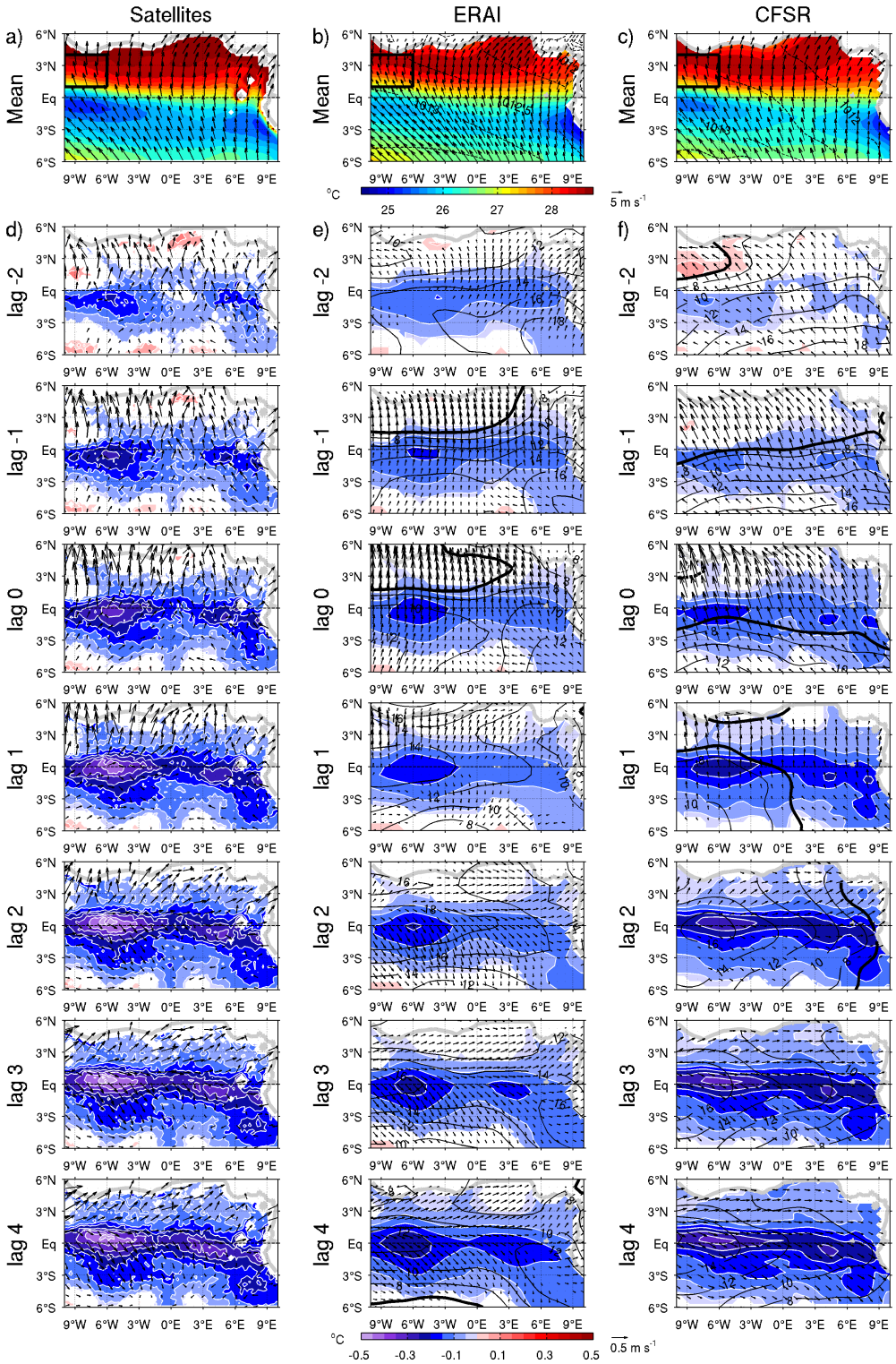

Figure 1. (a-c) Mean SST (colours, °C), SLP (contours, Pa) and surface wind (arrows, m s^{-1}) during May-June 2000-2009 and (d-f) lagged regressions of these anomaly fields onto the V-index (see text for more details) with TMI and QuikScat satellites (left), ERAI (centre) and CFSR (right). Only 10 % significant correlations are plotted. The reference series lags (leads) at the negative (positive). Lags in day step, from lag -2 to 4.

anomalous high SLP perfectly matches the cold SST pattern. Therefore, this mechanism is visibly at stake in the air-sea interaction dynamics of the Gulf of Guinea as well.

In summary, the SST front appears to be a key region for air-sea interaction in the Gulf of Guinea: large-scale wind fluctuations generate large equatorial SST anomalies, inducing SLP anomalies, which in turn modify the wind and, in particular, increase the southerlies between the equator and the coast.

For the present work, a focus is made on the impact of this air-sea interaction on the Guinean coast rainfall. Indeed, in spring and early summer, the seasonal rainfall belt is located around 1-10°N (Thorncroft *et al.* 2011). Moreover, some hints were shown in Leduc-Leballeur *et al.* (2011) that an

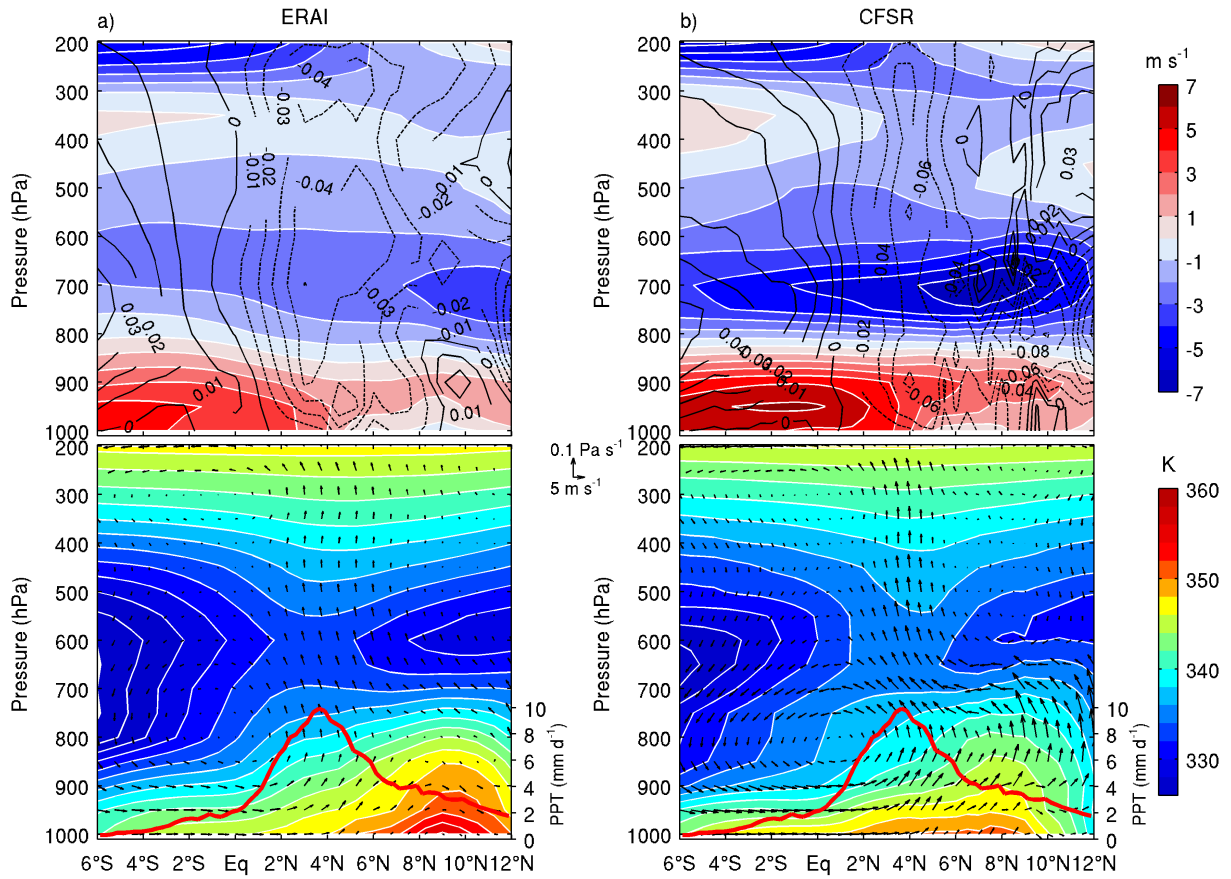

Figure 2. (top) Mean meridional wind (colours, m s^{-1}) and vertical velocity (contours, Pa s^{-1}). (bottom) Mean equivalent potential temperature (colours, K), meridional wind / vertical velocity (arrows) with (a) ERAI and (b) CFSR, as well as TRMM precipitation (red line, mm d^{-1}) during May-June 2000-2009 between 10-6°W.

equatorial SST cooling could influence the deep atmospheric convection in the north of the Gulf of Guinea. It is thus of particular interest to investigate the fluctuations of the Guinean coastal rainfall induced by an acceleration of surface oceanic southerlies in the vertical atmospheric circulation.

3.3. Atmospheric response

Figure 2 shows the mean vertical atmospheric profiles between 10°W and 6°W in May-June, in ERAI (a) and CFSR (b) (the vertical component of the velocity was strongly exaggerated for clarity).

The highest upward vertical velocity is found over the Guinean coast (around 5°N), along the whole atmospheric column (about -0.04 Pa s^{-1} in ERAI and -0.06 Pa s^{-1} in CFSR). At the same place, in the middle-low atmosphere (around 600 hPa), the largest potential equivalent temperature (Tep) is observed. Subsidence occurs over the ocean, south of the equator, at an average rate of 0.03 Pa s^{-1}. A low atmospheric local circulation (LALC hereafter) is visible under 600 hPa: the corresponding cell centre is found at 800 hPa around 1°S in ERAI and 1°N in CFSR on average, with an upper branch (maximal southward velocity) located around 700 hPa. Its southward winds reaches 2 m s^{-1} in ERAI (4 m s^{-1} in CFSR), but the northward winds of the lower branch are about 4 m s^{-1} in ERAI (6 m s^{-1} in CFSR). This LALC, together with the presence of the warm and dry air at about 600 hPa north of 5°N (associated to upper branch of the shallow meridional circulation or SMC; Zhang *et al.* (2008); Thorncroft *et al.* (2011)), explains why the deep atmospheric convection does not occur where the surface Tep is maximal (at 9°N, Figure 2b) but instead takes place further south, near the coast, where it is favoured by the coastal convergence of moist oceanic southerlies.

In order to investigate the link between the fluctuations of southerlies north of the equator and the deep coastal convection, lagged regressions were performed in the latitude-pressure section onto the same V-index as in the previous section (still in the 10-6°W meridional band). Figure 3 shows the resulting anomalous patterns from lag -2 to lag 2, *i.e.* the 2 days before and after a southerly burst, for meridional wind, vertical velocity and Tep with ERAI (a) and CFSR (b) as well as TRMM precipitation. The two reanalyses show similar patterns.

At lag -2 (*i.e.* 2 days before a maximal burst of southerlies), a slight intensification of the LALC is observed. The subsidence above the ocean increases, and the convection near the coast weakens. The next day (lag -1), the LALC strengthens, with a still increasing subsidence above the ocean and southerly wind north of the equator, together with a strong decrease in precipitation above the ocean, south of 4°N. In parallel, the Tep positive anomaly stretches in the low atmosphere north of 2°N, suggesting an accumulation of warm and wet air toward the coastal region. A small increase in the coastal precipitation (around 5°N) is observed as well, which implies that the deep convection has somewhat started to intensify;

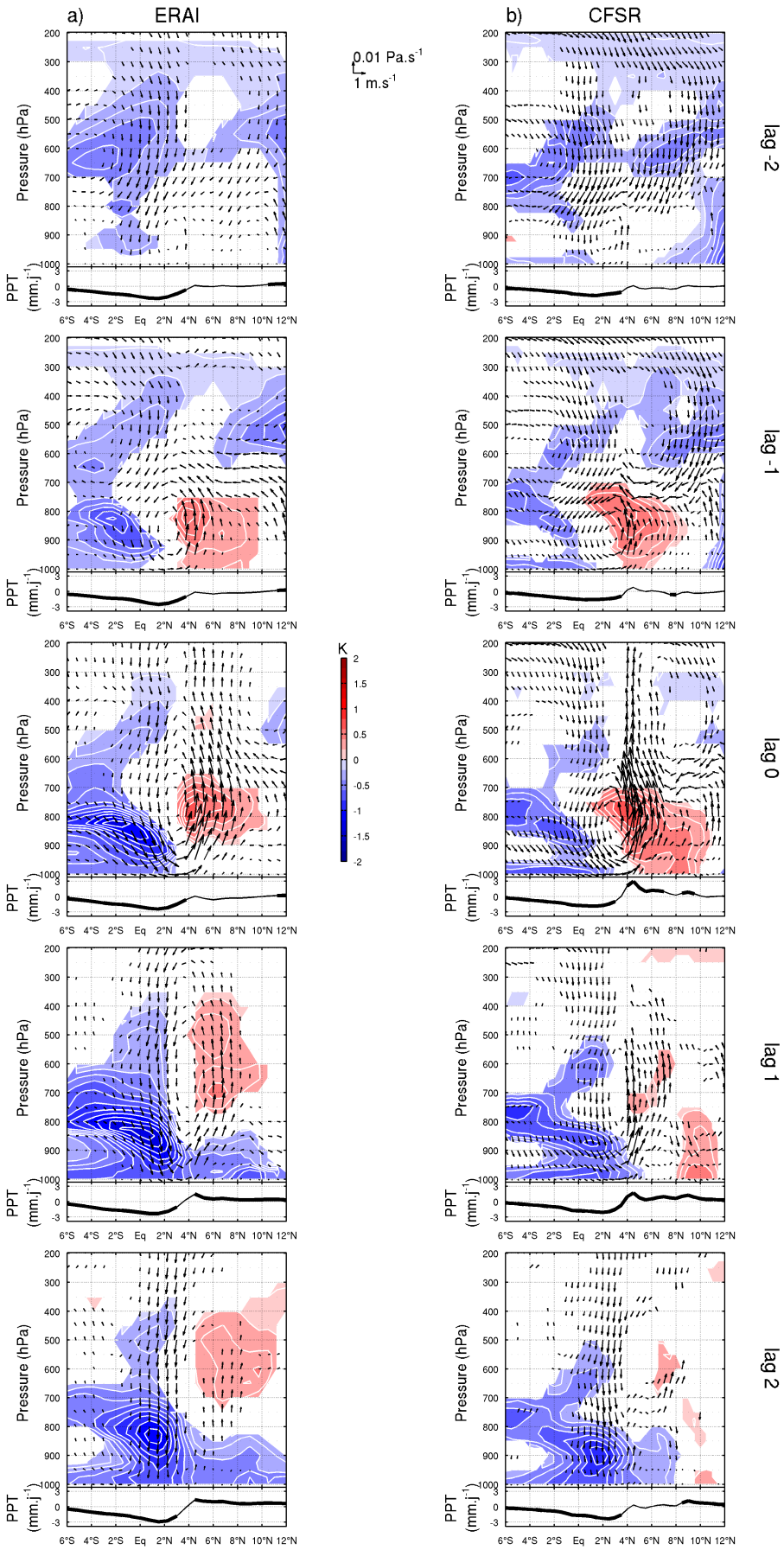

Figure 3. Lagged regressions of equivalent potential temperature (colours, K), meridional wind / vertical velocity (arrows) onto the V-index (see text for more details) with ERAI (a) and CFSR (b). Only 10 % significant correlations are plotted. Lagged regressions of TRMM precipitation (mm d^{-1}) are drawn in black line with 10 % significant correlations in heavy line. The reference series lags (leads) at the negative (positive). Lags in day step, from lag -2 to 2.

however, this effect is maximal the next day (at lag 0), when the southerlies between the equator and the coast (corresponding to the V-index) are the strongest, and the convection between 4°N and 8°N until 200 hPa is the most intense. South of 2°N, the subsidence increases, mainly below 700 hPa, where a strong Tep negative anomaly is also observed, together with a persistence of the decrease in precipitation south of 4°N.

At lag 1, the whole deep circulation is intensified (*i.e.* stronger than normal deep convection around the coast, and stronger than normal deep subsidence around the equator) and remains between the equator and 8°N. On the oceanic side, the Tep negative anomaly develops in altitude and stretches until the coast. On the coastal side, a Tep positive anomaly (albeit hardly significant in CFSR) persists above 800 hPa between 4°N and 8°N, together with a still-significant increased precipitation. Eventually, at lag 2, only a strong anomalous subsidence remains between the equator and the coast, still with a decrease in precipitation: anomalies in coastal deep convection and precipitation cannot be observed anymore.

In brief, a strengthening of the southerlies between the equator and the coast leads to an increased LALC in the region, transports moist air toward the coast, and warms up the continental Tep, favouring the conditions for deep convection and increasing rainfall around the coast.

3.4. Discussion

The lagged regressions in May-June 2000-2009 provide some information on the events preceding and following a surface wind strengthening north of the equator at the scale of a few days. The robustness of these results is very high, since they were found in different datasets: satellite measurements, and two reanalyses datasets. For the three datasets, a surface wind strengthening north of the equator is found to significantly result in a SST cooling along the equator (Figure 1). In the same way, the anomalous patterns of Tep, meridional wind and vertical velocity found in both reanalyses datasets are significant, albeit a faster disappearance of positive Tep anomalies and vertical velocity in the coastal region at lag 1 and 2 in CFSR (Figure 3). However, the SST cooling is weaker in the reanalyses than in the satellite observations, probably because of the low resolution in the models, which cannot take into account the small-scale oceanic dynamics and thus underestimates the SST variance at daily scales. This is however less true in the CFSR reanalyses, where the SST seems to be significantly more realistic at daily timescales, probably because the CFSR model resolution is higher, but also because it is a coupled ocean-atmosphere, and thus allows for the SST to react to the atmospheric fluctuations: this clearly emphasizes the interest of using coupled reanalyses to investigate the ocean-atmosphere interaction mechanisms.

In summary, a strengthening of the southerlies between the equator and the coast is linked to an increased LALC in the region. It transports moist air toward the coast, warming up the continental Tep, which creates favourable conditions for deep convection around the coast. Figure 4 sums up in a diagram our interpretation of the coupling events: a large-scale increase in South Atlantic / Gulf of Guinea southeasterlies (1) (*i.e.* corresponding to a stronger St Helena anticyclone, with a general increased subsidence in the whole region (2), that can be partially observed in Figure 3a and b) leads to an equatorial cooling of the SST (*i.e.* an intensification of the SST front (3)). As a result, and through the two mechanisms previously discussed:

- first, the MABL stabilises over the cold SST, resulting in the weakening of equatorial surface winds, while stronger than normal southerlies persist between the equator and the coast. The latter increase the coastal convergence (due to the frictional effect of the continent), while the resulting divergence around the equator favours a local subsidence: the LALC intensifies (4).
- second, an anomalous SLP gradient results from the anomalous SST gradient (with a high SLP anomaly over the cold equatorial SST anomaly) and also contributes to the intensification of the southerlies between the equator and the coast, *i.e.* of the LALC as well.

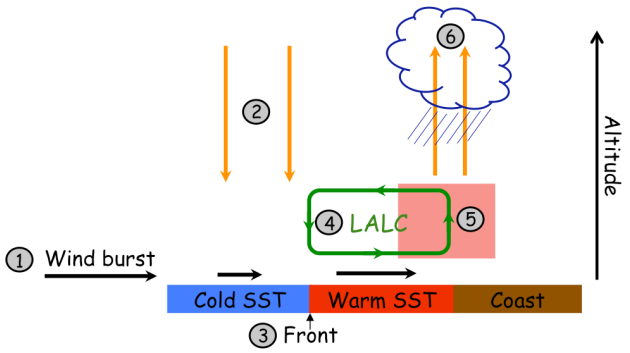

Figure 4. Schematic altitude-latitude section of southeastern wind burst (1) effects over the Gulf of Guinea on surface wind (black arrows), SST front (3), subsidence (2) / convergence (6) (orange arrows) and LALC (4) (green loop), which transports warm and wet air (5) (red rectangle) toward the coast.

This results in an increased advection of moisture in the lower LALC toward the coast, and thus a warmer coastal Tep (5), which favours the deep convection and increases the Guinean coastal rainfall (6). But meanwhile, the subsidence over the ocean has brought down a negative Tep anomaly, which inhibits the precipitation there, and carries it toward the coast. This damps the mechanism within a few days.

Note that all this was inferred from the linear regressions showed in Figure 1 and 3, so the reversed mechanisms are at work with initial weaker than normal southeasterlies in the Gulf of Guinea (*i.e.* southward displacement of the SST front, thus local equatorial SST warming, which will increase even more the equatorial surface wind and weaken southerlies between the equator and the coast, weakening the LALC, etc). Of course, non-linear responses are probably at work here, and could largely complicate the air-sea interaction mechanisms described here.

However, in West Africa, the precipitation is usually associated with westward convective systems, which interact with synoptic atmospheric disturbances such as the African Easterly Waves (AEW, Reed *et al.* (1977); Fink and Reiner (2003); Mathon *et al.* (2002)). Contrary to what is suggested here, the southerlies strengthening between the equator and the coast could be a result (and not the cause) of an increased coastal convection. In order to verify this hypothesis, linear regressions of TRMM precipitation and QuikScat surface

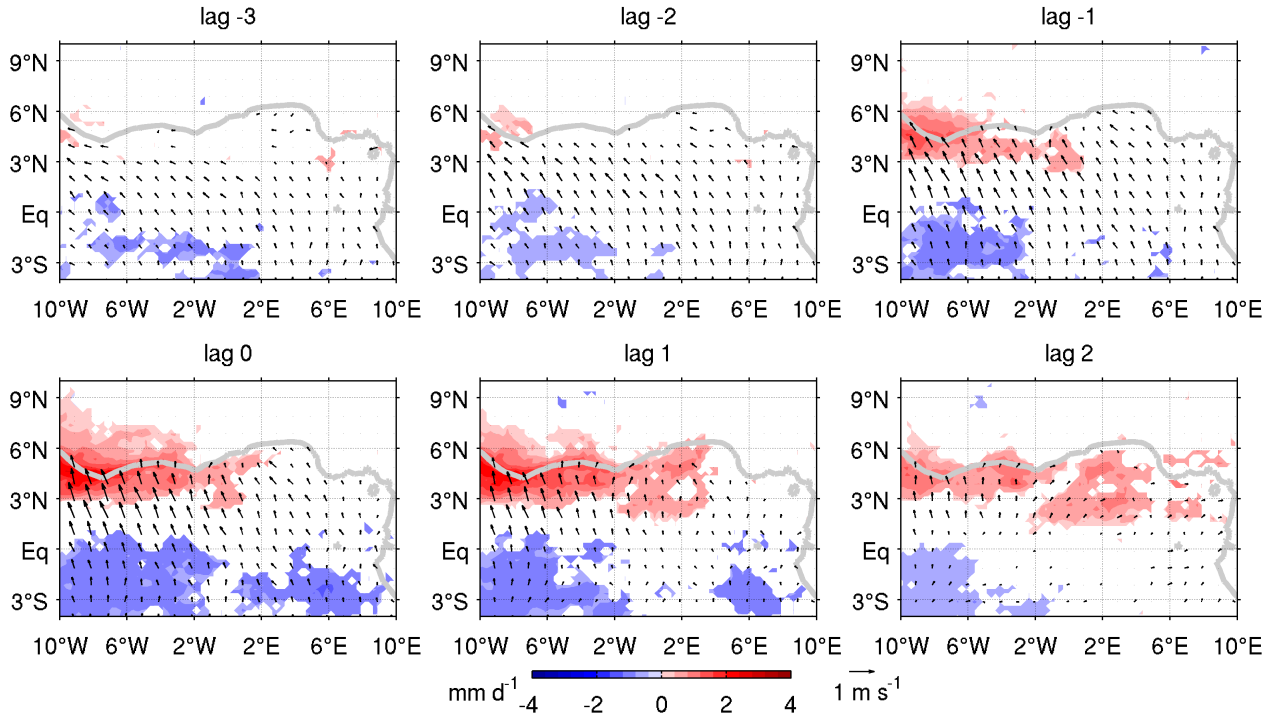

Figure 5. Lagged regressions of TRMM precipitation (colours, mm d^{-1}) and QuikScat surface wind (arrows, m s^{-1}) onto the V-index (see text for more details). Only 10 % significant correlations are plotted. The reference series lags (leads) at the negative (positive). Lags in day step, from lag -3 to 2.

wind on the V-index were analysed from lag -3 to lag 2 (Figure 5). At lag -3, the surface wind weakly increases north of the equator, and no significant precipitations anomaly is observed along the coast or above the continent. The positive precipitation anomaly appears at lag -2 and stretches along the coast from lag -1, when the surface wind strengthening reinforces north of the equator. At lag 0, the maximal surface wind strengthening is associated with a positive precipitation anomaly, maximum between 10°W and 2°E along the coast, and a precipitation negative anomaly south of the equator. Eventually, from lag 1 to 2, the surface wind strengthening persists, as well as the increased precipitation along the coast. No westward convective system (*i.e.* which would travel east-west during the time lags) is observed: the mechanism proposed by the previous statistical analysis seems to be a local process, acting along the coast on the precipitation. Of course, the AEW play an important role on Guinean coastal rainfall, but what is highlighted here is the significant influence of air-sea interaction in the Gulf of Guinea on its intraseasonal variability, which inserts in the seasonal evolution between the beginning of May and the end of June.

Similar regressions have been performed during the April-May and June-July period (not shown). They show that in April-May, the LALC is only present during an equatorial SST cooling and surface wind strengthening north of the equator, both generated by a southeastern wind burst. This circulation in the low atmosphere then disappears until the next wind burst. On the contrary, in June-July, the LALC is always present and the wind bursts intensify it. This suggests that a succession of wind bursts is needed to install the LALC, which favours, on a long-term basis, the convection at the coast. Moreover, Zheng *et al.* (1999) describe an albedo / rainfall / vegetation feedback leading the northward seasonal migration of the precipitation maximum in West Africa. From their model, they notice a decisive influence of the SST in the Gulf of Guinea on the beginning of this northward migration. A particularly strong equatorial SST cooling would induce a southerlies strengthening, increasing the coastal convergence and convection strongly enough to trigger the deep convection at a self-sustaining level. Linear regressions are obviously unable to emphasize the possible existence of such a decisive seasonal triggering event: it is thus investigated in the next section by using a different method.

4. Seasonal transition

The coastal phase is defined in Thorncroft *et al.* (2011) as the period when the precipitation maximum reaches the coastal region, but remains over the ocean. Nguyen *et al.* (2011) propose to define the onset of this phase as the moment when the precipitation stops south of the equator (below 2 mm d^{-1}). However, Sultan and Janicot (2003) define the "preonset" and "onset" of the West African monsoon, which can be assimilated respectively to the beginning and the ending of the coastal phase (as suggested by Nguyen *et al.* (2011)). The "preonset" corresponds to the beginning of the rainy season over the Sudano-Sahelian zone. The average date is 14 May (over the period 1968-90) and it is computed from the 925 hPa zonal wind at 15°N. The "onset" is linked to the abrupt latitudinal shift of the ITCZ, with an average date being 24 June (over the period 1968-90), computed from the daily rainfall. However, previous results show that there is probably a seasonal discontinuity inside this coastal phase, which makes these dates not sufficient to completely define this period.

Figure 6 shows the QuikScat surface wind averaged in April and July in the EEA. In April, north of the equator, the wind is globally homogeneous and clearly weaker than further south,

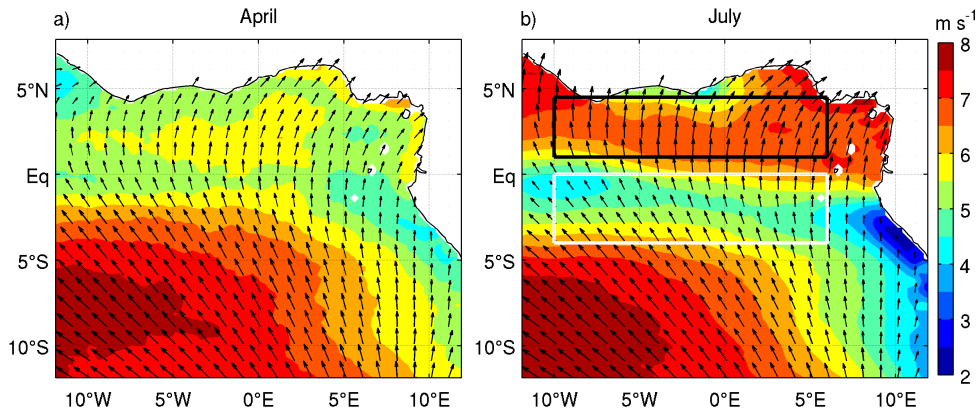

Figure 6. Mean QuikScat surface wind speed (m s^{-1}) in (a) April and (b) July 2000-2009. North Area in black box and Upwelling Area in white box.

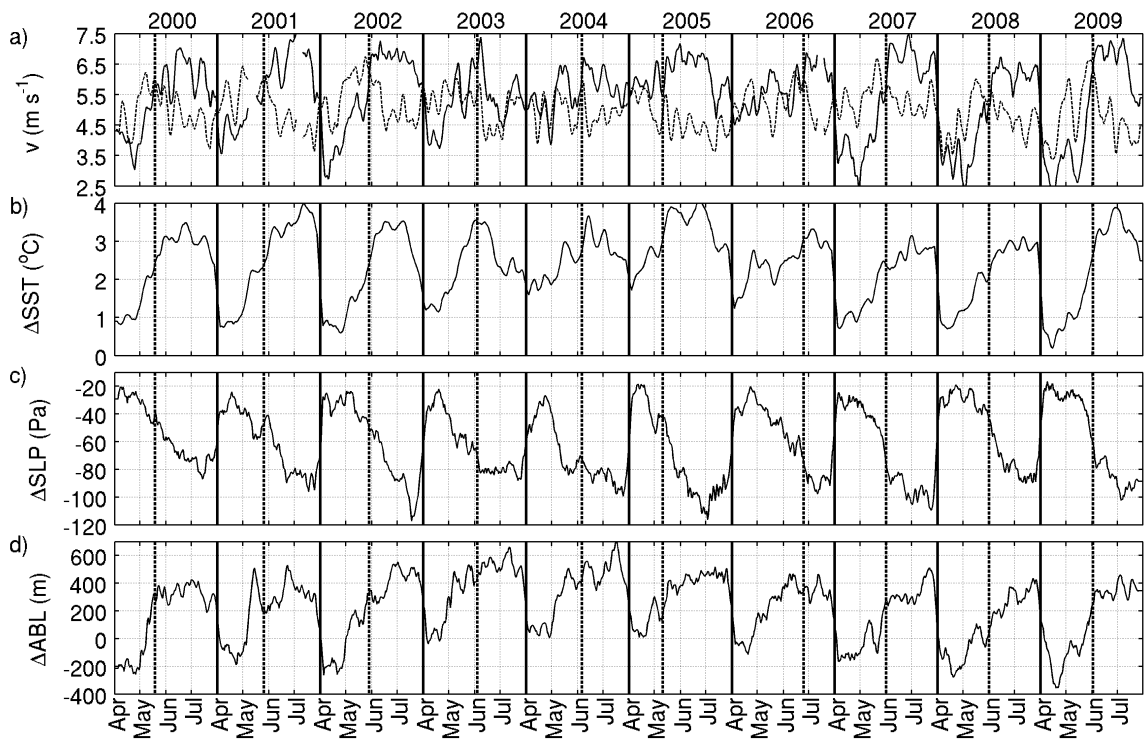

Figure 7. April-July time series of 2000-2009 years (a) mean meridional wind in the North (solid line) and Upwelling Area (dashed line) from QuikScat; differences between the North Area minus the Upwelling Area of (b) SST TMI (°C), (c) SLP ERAI (Pa) and (d) ABL computed from ERAI (m). The moving averages on 7 days are plotted to clarify the figure.

where the influence of the St Helena anticyclone can be felt. In July, the stronger winds globally observed in the region, due to the seasonal strengthening of the anticyclone shifted northward, are weakened along an equatorial band, which coincides with a cooler SST. Thus, a sharp change in the wind pattern of the Gulf of Guinea is observed before and after the coastal phase. In order to emphasize the specificity of such a change inside the spring and summer months, the period of investigation was extended from April to July (Figure 6), thereby increasing the contrast observed in the wind patterns between the beginning and the end of the period.

4.1. An abrupt wind change

Two key areas can be defined from these observations: the North Area (1-4.5°N/10°W-6°E; black box on Figure 6) with means of about 5.4 m s^{-1} in April and 6.6 m s^{-1} in July and the Upwelling Area (4°S-0°N/10°W-6°E; white box on Figure 6) with means of about 5.8 m s^{-1} in April and 5.2 m s^{-1} in July. The meridional band chosen in this part is 10°W-6°E, in order to index the whole EEA.

Figure 7a shows the meridional wind in the North and Upwelling Areas from April to July and for each year of the decade 2000-2009. In June, a sharp wind increase of about 2 m s^{-1} is generally observed in the North Area, when it becomes stronger than the wind in the Upwelling Area. The difference between the North and Upwelling Areas located from either side of the SST front exhibits marked changes as well at about the same time (Figure 7b-d). Indeed, SST between North and Upwelling Areas increases by 2°C, which suggests a sharp intensification of the SST front. In parallel, the differences in SLP increase by 50 Pa and in atmospheric

boundary layer (ABL) height by 500 m. These variations are in agreement with the mechanisms proposed by Lindzen and Nigam (1987) and Wallace *et al.* (1989) around a SST front, which suggest a lower SLP and a higher ABL above warm SST (here North Area) than cold SST (here Upwelling Area). Thus, this implies a link between the meridional wind strengthening and the SST front intensification in the oceanic and atmospheric boundary layers.

In order to emphasize this dramatic strengthening in the North Area wind and represent its timing, a reference date is defined for each year. As the latter coincides with a concomitant weakening of the Upwelling Area wind, the date is chosen as the time when the wind in the North Area becomes, and then remains, stronger than in the Upwelling Area (Figure 7a) in April-June. In average, this phenomenon occurs on the 31 May, with two extremes in 2005 (12 May) and 2006 (26 June). From this reference date (thereafter noted as t_0), a wind surface composite is computed.

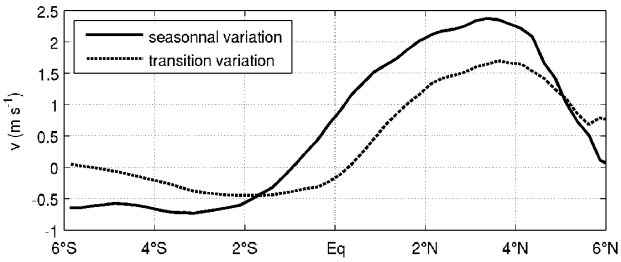

Figure 8. Seasonal and transition variation of QuikScat meridional surface wind variation averaged between 10°W-6°E for 2000-2009 (see text for computing details).

To understand the impact of this transition, it needs to be compared to the seasonal evolution. Therefore, the seasonal variation is computed as the mean 15 first days of July minus the mean 15 last days mean of April and the variation during the transition as the mean 15 days after minus the mean 15 days before t_0. Figure 8 compares this seasonal variation with the transition variation, both averaged for the 2000-2009 period, in the 10°W-6°E band for the QuikScat meridional surface wind. The seasonal variation shows a decrease in meridional surface wind about 0.5 m s^{-1} south of 2°S and an increase north of the equator (up to 2.5 m s^{-1} around 3°N). Figure 8 suggests that, in 4°S-2°S band and 1°N-4°N band, more than two thirds of the seasonal variation takes place during the transition period, whereas this period represents only a third of the whole duration (between 15 last days of April and 15 first days of July). For example, the variation during the transition at 3°N is about 1.5 m s^{-1}, compared to less than 2.5 m s^{-1} for the seasonal variation at this place. Thus, this seasonal transition seems to be a major phenomenon in the seasonal evolution of the region.

4.2. Analysis of the seasonal transition

Lagged composites are then computed around the reference date t_0 by averaging the fields from lag -15 (15 days before t_0) to lag 15 (15 days after, Figure 9a-b) for the 2000-2009 period, on the 10-6°W meridional band with satellite products. Before t_0 (at negative lags), the sharp wind accelerations are mostly confined south of 4°N. The region south of equator is colder than north, with a SST front centred at 1°N. At lag 0 (t_0), a wind stronger than 8.5 m s^{-1} is observed in the southern part of the domain. It weakens about the equator down to 6.5 m s^{-1}, before strengthening again north of 4.5°N. SST decreases, particularly south of the equator. In the following lags, the wind remains strong north of the equator (> 7 m s^{-1}) and weak south of the equator (< 5.5 m s^{-1}). The SST gradient between the equator and 2°N is stronger, about 3°C. The map of differences between the averaged 15 days after and 15 days before t_0 confirms that the previous observation is robust over the whole region (6°S-6°N/10°W-6°E, Figure 9c-d). The wind strengthens by about 1 m s^{-1} in the North Area and weakens by about 0.3 m s^{-1} in the Upwelling Area. In the same time, SST cools by more than 3°C around the equator and about 1°C north of 2°N, which highlights the intensification of SST front about 1°N.

Coinciding changes in the whole atmosphere are investigated by computing composite sections (*i.e.* the mean 15 days after and before t_0) of the relative humidity and wind in the vertical along the meridional section 10-6°W with ERAI and CFSR (Figure 10), which both agree. Before t_0, a moist boundary layer (> 70 %) is observed in the low atmosphere. It stretches up to 850 hPa above the ocean but is thicker north of 2°N (up to 800 hPa). The LALC is visible between 1000 and 600 hPa, centred over the equator at 800 hPa. Deep convection occurs between 2°N and 7°N with mean vertical wind speed of about -0.04 Pa s^{-1}, carrying humidity upward, while subsidence takes place south of 2°N with a mean vertical wind speed almost zero at the equator. After t_0, the moist boundary layer is thinner above the equator (about 900 hPa) but thicker (about 750 hPa) and moister (> 90 % below 850 hPa) north of 2°N. The LALC has clearly shifted northward and is now centred about 2°N at 850 hPa. The subsidence above the ocean has intensified (with a downward wind of about 0.03 Pa s^{-1} between 6°S and 2°N) and the humidity has decreased by about 6 %. The deep convection is stronger (with an upward speed of about -0.05 Pa s^{-1} at 5°N) and is now confined between 4-8°N.

Thus, most of the characteristics linked with a southerlies strengthening event found in the previous section are found again in these composites (Figure 9 and Figure 10), *i.e.* increased equatorial divergence / subsidence (with less precipitation) and coastal convergence / convection (with increased precipitation). This shows that the criteria used to choose the reference date was pertinent, as it catches the intraseasonal signal as well as the seasonal discontinuity.

4.3. Impact on precipitation

These atmospheric changes seem to strongly impact the precipitation distribution. Figure 11a shows the lagged precipitation composite around t_0 in the 10°W-6°W meridional band. Before t_0, the precipitation broadly stretches until the equator and even south of it. At t_0, the precipitation is concentrated north of 2°N with a maximum of about 9 mm d^{-1} at 4°N and drops to zero south of 2°N. In the following lags, the maximum of precipitation stays at about 4°N and no more precipitation is observed south of 2°N. According to the difference map between the averaged 15 days after and 15 days before t_0 (Figure 11b), the precipitation increases by about 2 mm d^{-1} north of 4°N and decreases by up to 3 mm d^{-1} between the equator and 4°N.

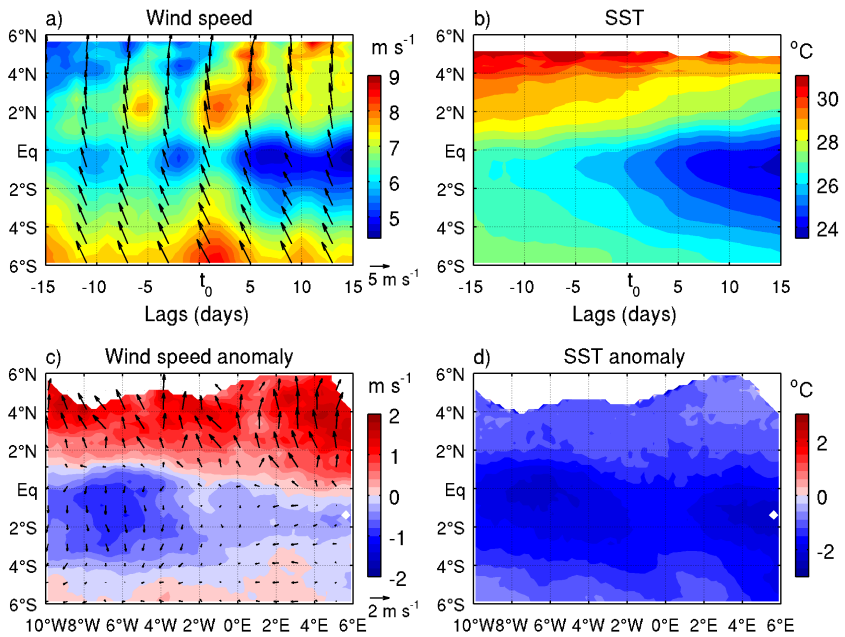

Figure 9. (a-b) Composites computed from t_0 of each year (2000-2009), in average between 10-6°W and (c-d) difference maps between the mean composite of 15 days after t_0 minus the mean composite of 15 days before t_0 for (left) QuikScat wind speed (m s^{-1}) and (right) TMI SST (°C).

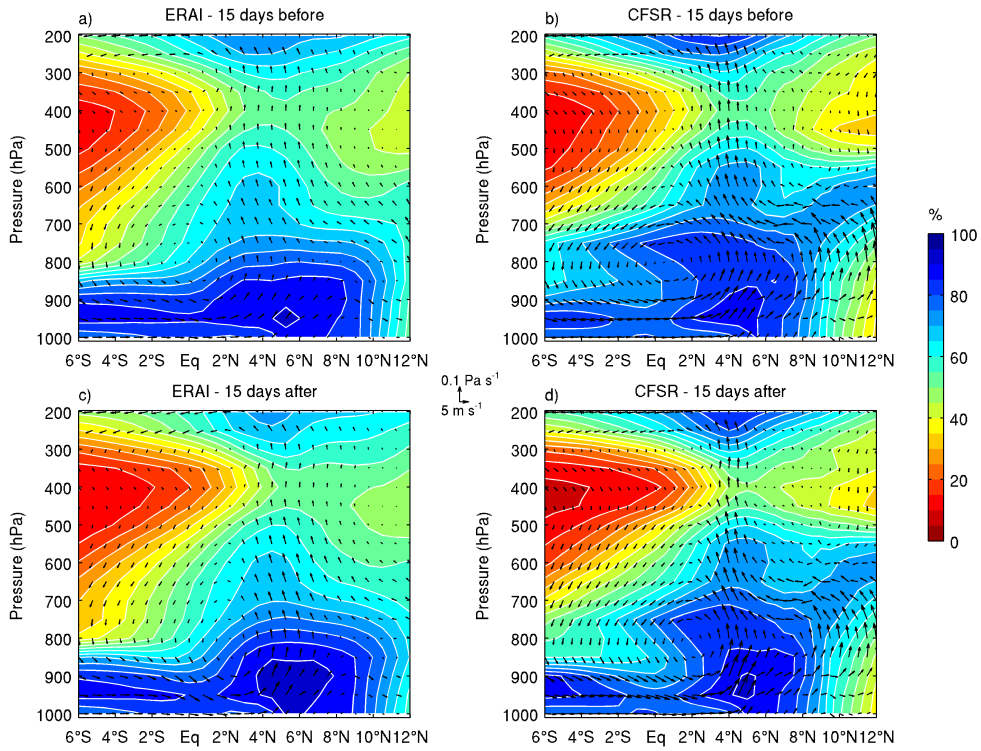

Figure 10. Mean composites of (a-b) 15 days before t_0 and (b-c) 15 days after t_0, in average between 10-6°W for the relative humidity (colours, %) and meridional wind / vertical velocity (arrows) with ERAI (left) and CFSR (right).

To compare this evolution during the transition with the seasonal evolution, but being free of the effect of strong systems on the precipitation composite, the daily precipitation occurrences are counted during the 15 last days of April and the 15 first days of July minus (Figure 11c) and during the 15 days before and the 15 days after t_0 (Figure 11d). The end of April is the very beginning of the coastal phase of the West African monsoon and there is significant precipitation over the ocean. However, the precipitation maximum is located between 2°N and 4°N. In comparison, during the 15 days before t_0, this maximum is always located at this place. In the beginning of July, the precipitation maximum stands around 6°N. In comparison, during the 15 days after t_0, this maximum is located between 4°N and 6°N. Thus, the transition seems to influence the northward seasonal

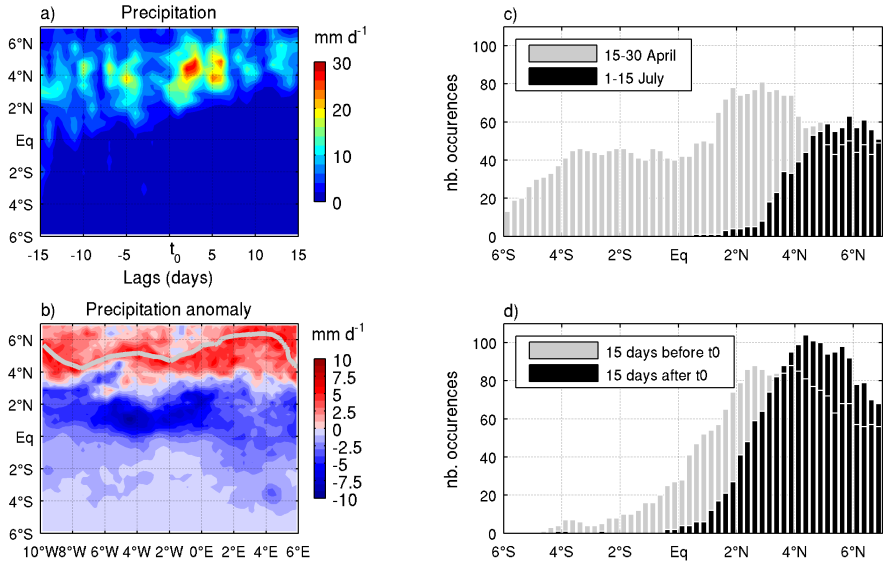

Figure 11. (a) Composites computed from t_0 of each year (2000-2009), in average between 10-6°W. (b) Difference maps between the mean composite of 15 days after t_0 minus the mean composite of 15 days before t_0 for TRMM precipitations (mm d^{-1}). (c) TRMM daily precipitation occurrences during the 15 last days of April (grey bars) and the 15 first days of July (black bars). (d) TRMM daily precipitation occurrences during the 15 days before t_0 (grey bars) and the 15 days after t_0 (black bars). An occurrence is define as a daily precipitation higher than 5 mm d^{-1} averaged between 10-6°W.

migration of the precipitation band, which shows an abrupt shift by 2° within 15 days.

To confirm these observations, a qualitative indicator of production or decrease of CAPE (Convective Available Potential Energy) is used ("CAPE tendency" hereafter). However, it must be noted that this quantity does not correspond to the exact CAPE tendency, and should be considered as a qualitative estimate. Protat and Lemaître (2001) suggest that the CAPE tendency can be estimated from the rate of change of the vertical Tep gradient using the following equation:

$$\frac{\partial}{\partial t}\left(\frac{\partial \mathrm{Tep}}{\partial z}\right) = \underbrace{-u\frac{\partial}{\partial x}\left(\frac{\partial \mathrm{Tep}}{\partial z}\right) - v\frac{\partial}{\partial y}\left(\frac{\partial \mathrm{Tep}}{\partial z}\right) - w\frac{\partial}{\partial z}\left(\frac{\partial \mathrm{Tep}}{\partial z}\right)}_{\text{classic advection}} \underbrace{-\frac{\partial u}{\partial z}\frac{\partial \mathrm{Tep}}{\partial x} - \frac{\partial v}{\partial z}\frac{\partial \mathrm{Tep}}{\partial y} - \frac{\partial w}{\partial z}\frac{\partial \mathrm{Tep}}{\partial z}}_{\text{differential advection}} \quad (1)$$

The negative values are associated with a CAPE supply and the positive values with a CAPE loss.

Figure 12a-b show lagged composites of the CAPE tendency field computed with ERAI and CFSR around t_0 from lag -15 to lag 15 for the same meridional band (10-6°W). Before t_0, the CAPE tendency exhibits a positive (negative) area south (north) of about 2°N. After t_0, the positive area increases and stretches as far as 5°N. To explain these variations, the sum of the "classic" and differential advection is computed for zonal, meridional and vertical components. Figure 12c-d represents the meridional advection with ERAI and CFSR. It is the meridional advection term, which mainly leads the CAPE tendency in the whole region, whereas the vertical advection term leads about 6°N and the zonal advection term is weak in comparison with both previous terms (not shown).

Before t_0, south of 2°N, the CAPE loss is due to the meridional wind which moves the CAPE northward (Figure 12c-d). This contributes to settle a stable atmosphere above the ocean in agreement with the SST cooling and the subsidence observed in the previous section. This CAPE meridional advection constitutes a CAPE supply for the vertical advection between 2°N and the coast (not shown) and suggests that the convection can develop there. Thus, the precipitation is weak south of 2°N, but stronger from 2°N to the coast, where the convection is favoured in agreement with Figure 10.

After t_0, southerlies increase north of the equator and move the CAPE as far as about 4°N. It results in a concentration of CAPE between 4°N and 6°N which can feed the vertical advection. Between 2°N and the equator, the CAPE loss by meridional advection is coherent with the stabilisation of the atmosphere observed on Figure 10 through the increase in subsidence and the decease in humidity.

Thus, this increase in available CAPE associated with the intensification of the subsidence south of 2°N (Figure 10), agrees with the migration of precipitation toward the coast observed during the seasonal transition (Figure 11).

5. Conclusion

The air-sea interaction mechanisms playing a role in the coastal precipitation of the Gulf of Guinea are investigated from satellite measurements and reanalyses datasets (ERAI and CFSR). The focus is made on the wind strengthening events north of the equator, particularly interesting because of their link with the air-sea interaction in the EEA and their impact on the tropospheric dynamics through the convection along the Guinean coast. Regression analyses were performed to study the origin of this wind acceleration and their effect north of the equator, in May-June 2000-2009.

During boreal spring, southeasterlies intensify in the EEA due to the seasonal variability of the St Helena anticyclone (Marin *et al.* 2009; de Coëtlogon *et al.* 2010; Caniaux *et al.* 2011). This leads to a SST cooling south of the equator, which weakens the overlying southeasterlies, in agreement with the negative feedback proposed in de Coëtlogon *et al.* (2010). Due to the cold SST south of equator and warm SST north of the

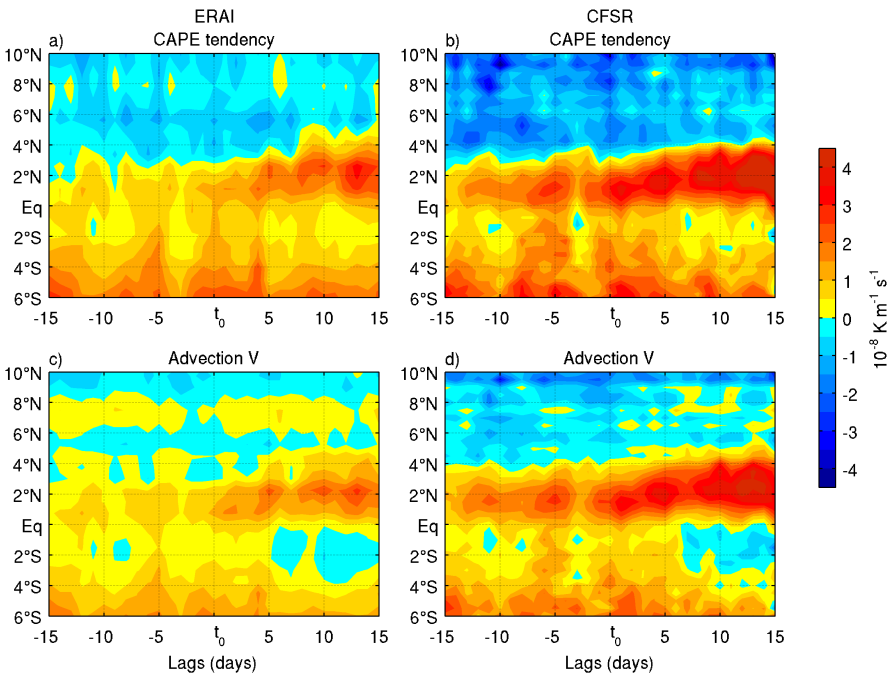

Figure 12. Mean composites computed from t_0 of each year between 10-6°W of (a-b) the CAPE tendency field and the (c-d) meridional advection term contributing to the CAPE tendency with ERAI (left) and CFSR (right).

equator, an equatorial surface wind divergence is combined with an increased coastal convergence to intensify the low atmospheric local circulation (LALC). In parallel, a cross-equatorial pressure gradient develops and also contributes to the surface wind strengthening between the equator and the Guinean coast. This confirms that the wind surface strengthening results from the air-sea interaction trough the equatorial SST front, as suggested in Leduc-Leballeur *et al.* (2011) for the 2006 season. This mechanism transports moisture in the Gulf of Guinea toward the coast, which increases the coastal convection and favours a deep circulation between the ocean and the coast: the coastal precipitation is thus intensified during one or two days. In short, a wind burst in the Gulf of Guinea releases a mechanism, which lasts for about four days and supports the coastal convective activity through an equatorial SST cooling and a surface wind strengthening between the equator and the coast.

Nevertheless, the atmospheric circulation changes between May and June. In May, the LALC appears briefly, due to a southeastern wind burst, and collapses within a few days; whereas in June, the LALC is always active, and intensifies even more during the wind bursts. This suggests an abrupt seasonal transition prepared by a succession of southeastern wind bursts, and possibly triggered by a significantly stronger southeastern wind burst. This is accompanied by an abrupt change in the surface wind pattern as well: at the beginning of the coastal phase, the surface wind north of the equator is weaker than south of the equator, but subsequently the surface wind strengthens north of the equator and weakens south of the equator. A reference date can be defined as the transition between the two wind patterns, when the wind north of the equator becomes and remains stronger than south of the equator. The average date is the 31 May over the decade 2000-2009. This reference date gives a useful mark to investigate the intraseasonal processes installing the precipitation at the coast and completes the steps of the West African monsoon evolution proposed by some previous authors (*e.g.* Sultan and Janicot 2003; Nguyen *et al.* 2011).

The analysis of composites computed over the 10 years using the reference date shows that the transition is initially triggered by strong southeasterlies south of 4°S. The atmosphere is impacted as previously described, *i.e.* with an increased subsidence above the ocean and convection at the coast, as part of an intensified LALC and deep circulation upon the whole troposphere. These changes are sustained after the reference date: following the strengthening of the deep circulation, the LALC moves suddenly northward, releasing its feedback on the southerlies between the equator and the coast as a permanent situation, and the convective activity is intensified.

Moreover, these strong southerlies contribute to push the CAPE from the Gulf of Guinea toward the coast by meridional advection, feeding the coastal deep convection. This suggests that the Gulf of Guinea plays a key role in the energy and humidity supply of the coastal precipitation. Note that a strong influence of the SST front fluctuations in forcing the LACL fluctuations has been emphasized throughout this work. However, this hypothesis was only based on the analysis of the linear regression patterns: only sensitivity modelling experiments could definitively prove that statement, and quantify the effect of this mechanism.

Finally, this study suggests that a succession of wind bursts from the St Helena anticyclone can cause a sharp and durable change in the atmospheric circulation in the northern Gulf of Guinea, which leads to the concentration of precipitation at the coast during boreal spring by interacting with the northern front of the cold tongue. Caniaux *et al.* (2011) suggested that the equatorial SST cooling plays a role in the West African monsoon onset: in this framework, it would be interesting to investigate if the end of the Guinean coastal rainfall (rapidly

followed by the West African monsoon onset) could be due to a similar mechanism of air-sea interaction.

Acknowledgements

Based on a French initiative, AMMA was built by an international scientific group and is currently funded by a large number of agencies, including those in France, the UK, USA and Africa. It has been the beneficiary of a major financial contribution from the European Community's Sixth Framework Research Programme. Detailed information on scientific coordination and funding is available on the AMMA International website (http://www.amma-international.org). TMI data are sponsored by the NASA Earth Science MEaSUREs DISCOVER Project and QuikScat data by the NASA Ocean Vector Winds Science Team. The authors wish to thank G. Caniaux, S. Janicot and A. Weill for their help, as well as the reviewers for their constructive remarks.

References

Businger JA, Shaw WJ. 1984. The response of the marine boundary layer to mesoscale variations in sea-surface temperature. *Dyn. Atm. Oceans* **8**(3-4): 267–281, doi:10.1016/0377-0265(84)90012-5.

Caniaux G, Giordani H, Redelsperger JL, Guichard F, Key E, Wade M. 2011. Coupling between the Atlantic cold tongue and the west african monsoon in boreal spring and summer. *J. Geophys. Res.* **116**(C04003), doi: 10.1029/2010JC006570.

de Coëtlogon G, Janicot S, Lazar A. 2010. Intraseasonal variability of the ocean - atmosphere coupling in the Gulf of Guinea during boreal spring and summer. *Q. J. R. Meteorol. Soc.* **136**(Sp. Iss. SI Suppl. 1): 426–441, doi: 10.1002/qj.554.

Dee DP, Uppala SM, Simmons AJ, Berrisford P, Poli P, Kobayashi S, Andrae U, Balmaseda MA, Balsamo G, Bauer P, Bechtold P, Beljaars ACM, van de Berg L, Bidlot J, Bormann N, Delsol C, Dragani R, Fuentes M, Geer AJ, Haimberger L, Healy SB, Hersbach H, Hólm EV, Isaksen L, Kållberg P, Köhler M, Matricardi M, McNally AP, Monge-Sanz BM, Morcrette JJ, Park BK, Peubey C, de Rosnay P, Tavolato C, Thépaut JN, Vitart F. 2011. The era-interim reanalysis: configuration and performance of the data assimilation system. *Q. J. R. Meteorol. Soc.* **137**(656): 553–597, doi:10.1002/qj.828.

Fink A, Reiner A. 2003. Spatiotemporal variability of the relation between african easterly waves and west african squall lines in 1998 and 1999. *J. Geophys. Res* **108**(D11): 4332.

Friehe CA, Shaw WJ, Rogers DP, Davidson KL, Large WG, Stage SA, Crescenti GH, Khalsa SJS, Greenhut GK, Li F. 1991. Air-sea fluxes and surface layer turbulence around a sea surface temperature front. *J. Geophys. Res.* **96**(C5): 8593–8609.

Giordani H, Caniaux G. 2011. Diagnosing vertical motion in the equatorial atlantic. *Ocean Dynamics* **1**: 233, doi:10.1007/s10236-011-0467-7.

Gu G, Adler R. 2004. Seasonal evolution and variability associated with the west african monsoon system. *J. Clim.* **17**(17): 3364–3377.

Hashizume H, Xie SP, Fujiwara M, Shiotani M, Watanabe T, Tanimoto Y, Liu WT, Takeuchi K. 2002. Direct observations of atmospheric boundary layer response to sst variations associated with tropical Instability waves over the eastern equatorial pacific. *J. Clim.* **15**(23): 3379–3393, doi:10.1175/1520-0442(2002)015.

Huffman GJ, Bolvin DT, Nelkin EJ, Wolff DB, Adler RF, Gu G, Hong Y, Bowman KP, Stocker EF. 2007. The trmm multisatellite precipitation analysis (tmpa): Quasi-global, multiyear, combined-sensor precipitation estimates at fine scales. *Journal of Hydrometeorology* **8**(1): 38–55.

Kwon B, Benech B, Lambert D, Durand P, Druilhet A, Giordani H, Planton S. 1998. Structure of the marine atmospheric boundary layer over an oceanic thermal front: SEMAPHORE experiment. *J. Geophys. Res.* **103**(C11): 25 159–25 180.

Leduc-Leballeur M, Eymard L, de Coëtlogon G. 2011. Observation of the marine atmospheric boundary layer in the gulf of guinea during the 2006 boreal spring. *Q. J. R. Meteorol. Soc.* **137**(657): 992–1003, doi: 10.1002/qj.808.

Li T, Philander S. 1997. On the seasonal cycle of the equatorial atlantic ocean. *J. Clim.* **10**(4): 813–817, doi:10.1175/1520-0442(1997)010<0813:OTSCOT>2.0.CO;2.

Lindzen RS, Nigam S. 1987. On the role of sea surface temperature gradients in forcing low-level winds and convergence in the tropics. *J. Atmos. Sci.* **44**(17): 2418–2436.

Liu WT, Xie X, Polito PS, Xie SP, Hashizume H. 2000. Atmospheric manifestation of tropical instability wave observed by quikscat and tropical rain measuring mission. *Geophys. Res. Lett.* **27**(16): 2545–2548, doi: 10.1029/2000GL011545.

Marin F, Caniaux G, Bourlès B, Giordani H, Gouriou Y, Key E. 2009. Why were sea surface temperatures so different in the eastern equatorial Atlantic in june 2005 and 2006? *J. Phys. Oceanogr.* **39**(6): 1416–1431, doi: 10.1175/2008JPO4030.1.

Mathon V, Laurent H, Lebel T. 2002. Mesoscale convective system rainfall in the sahel. *Journal of applied meteorology* **41**(11): 1081–1092, doi:1520-0450(2002)041<1081:MCSRIT>2.0.CO;2.

McCreary J, Picaut J, Moore D. 1984. Effects of the remote annual forcing in the eastern tropical atlantic ocean. *J. Mar. Res.* **42**: 45–81.

Mitchell T, Wallace J. 1992. The annual cycle in equatorial convection and sea surface temperature. *J. Clim.* **5**(10): 1140–1156.

Nguyen H, Thorncroft C, Zhang C. 2011. Guinean coastal rainfall of the west african monsoon. *Q. J. R. Meteorol. Soc.* **137**(660): 1828–1840, doi: 10.1002/qj.867.

Okumura Y, Xie S. 2004. Interaction of the Atlantic equatorial cold tongue and the african monsoon. *J. Clim.* **17**(18): 3589–3602.

Peter AC, Le Hénaff M, Du Penhoat Y, Menkes C, Marin F, Vialard J, Caniaux G, Lazar A. 2006. A model study of the seasonal mixed layer heat budget in the equatorial atlantic. *J. Geophys. Res.* **111**(C6): C06 014, doi: 10.1029/2005JC003157.

Protat A, Lemaître Y. 2001. Scale interactions involved in the initiation, structure, and evolution of the 15 december 1992 mcs observed during toga coare. part i: Synoptic-scale processes. *Mon. Wea. Rev.* **129**(8): 1757–1778.

Reed R, Norquist D, Recker E. 1977. The structure and properties of african wave disturbances as observed during phase iii of gate12. *Mon. Wea. Rev.* **105**: 317–333, doi:10.1175/1520-0493(1977)105<0334:TEOAWD>2.0.CO;2.

Saha S, Moorthi S, Pan H, Wu X, Wang J, Nadiga S, Tripp P, Kistler R, Woollen J, Behringer D, *et al.* 2010. The ncep climate forecast system reanalysis. *Bull. Am. Meteorol. Soc.* **91**(8): 1015–1057, doi:10.1175/2010BAMS 3001.1.

Small RJ, deSzoeke SP, Xie SP, O'Neill L, Seo H, Song Q, Cornillon P, Spall M, Minobe S. 2008. Air sea interaction over ocean fronts and eddies. *Dyn. Atm. Oceans* **45**(3-4): 274–319, doi:10.1016/j.dynatmoce.2008.01.001.

Sultan B, Janicot S. 2003. The west african monsoon dynamics. Part II: The "preonset" and "onset" of the summer monsoon. *J. Clim.* **16**(21): 3407–3427.

Sweet W, Fett R, Kerling J, La Violette P. 1981. Air-sea Interaction effects in the lower troposphere across the north wall of the gulf stream. *Mon. Wea. Rev.* **109**(5): 1042–1052.

Thorncroft CD, Nguyen H, Zhang C, Peyrille P. 2011. Annual cycle of the west african monsoon: Regional circulations and associated water vapour transport. *Q. J. R. Meteorol. Soc.* **137**: 129–147, doi:10.1002/qj.728.

Vizy E, Cook K. 2001. Mechanisms by which Gulf of Guinea and eastern north Atlantic sea surface temperature anomalies can influence african rainfall. *J. Clim.* **14**(5): 795–821.

Wallace JM, Mitchell TP, Deser C. 1989. The influence of sea-surface temperature on surface wind in the eastern equatorial pacific: seasonal and interannual variability. *J. Clim.* **2**(12): 1492–1499.

Wentz FJ. 1997. A well-calibrated ocean algorithm for special sensor microwave / imager. *J. Geophys. Res.* **102**(C4): 8703–8718, doi: 10.1029/96JC01751.

Wentz FJ, Gentemann C, Smith D, Chelton D. 2000. Satellite measurements of sea surface temperature through clouds. *Science* **288**(5467): 847 – 850, doi:10.1126/science.288.5467.847.

Xie S, Carton J. 2004. Tropical atlantic variability: Patterns, mechanisms, and impacts. *Earth's Climate: The Ocean-Atmosphere Interaction, Geophys. Monogr* **147**: 121–142.

Xie SP. 2004. Satellite observations of cool ocean-atmosphere interaction. *Bull. Am. Meteorol. Soc.* **85**(2): 195–208.

Zhang C, Nolan DS, Thorncroft CD, Nguyen H. 2008. Shallow meridional circulations in the tropical atmosphere. *J. Clim.* **21**(14): 3453–3470, doi: 10.1175/2007JCLI1870.1.

Zheng X, Eltahir EAB, Emanuel KA. 1999. A mechanism relating tropical atlantic spring sea surface temperature and west african rainfall. *Q. J. R. Meteorol. Soc.* **125**(556): 1129–1163, doi:10.1002/qj.1999.49712555604.